



Vapor detection enabled by self-assembled colloidal photonic crystals

Hongta Yang^a, Peng Jiang^{a,*}, Bin Jiang^b

^a Department of Chemical Engineering, University of Florida, Gainesville, FL 32611, United States

^b Department of Mathematics and Statistics, Portland State University, Portland, OR 97201, United States

ARTICLE INFO

Article history:

Received 14 July 2011

Accepted 21 December 2011

Available online 2 January 2012

Keywords:

Photonic crystals
Self-assembly
Vapor condensation
Bragg diffraction
Vapor detection

ABSTRACT

Here we report the sensitive and reversible detection of vapors by using self-assembled colloidal photonic crystals. The condensation of various vapors in the interstitials of silica colloidal photonic crystals leads to red-shift and amplitude reduction of optical stop bands. A linear relationship between wavelength shift and vapor partial pressure has been observed for a variety of vapors including ethanol, water, and toluene. Importantly, the sensitivity of colloidal photonic crystal-based vapor detectors can be improved by nearly two orders of magnitude by using a new full-peak analysis technique that takes advantage of the manifest amplitude reduction of optical stop bands during vapor condensation. Optical simulation based on a scalar-wave approximation model shows that the predicted optical responses during vapor condensation in colloidal photonic crystals agree well with experimental results. The condensation of vapors between submicrometer-scale microspheres, a topic that has received little examination, has also been investigated by both experiments and theoretical calculations. Predictions based on a modified Kelvin equation match with the experiments for a wide range of vapor partial pressures.

Published by Elsevier Inc.

1. Introduction

Photonic crystals, also known as photonic band gap materials, are periodic dielectric structures with a forbidden gap for electromagnetic waves, analogous to the electronic band gap in semiconductors that lies at the heart of silicon technology [1–2]. Exemplified by gemstone opals, three-dimensional (3-D) photonic crystals are readily available by spontaneous crystallization of colloidal microspheres [3–10], making them a fertile test-bed for investigating new concepts and devices based on tunable structural colors [11–15]. A large variety of applications, such as diffractive optical devices (e.g., optical filters and switches) [7,16–18], chemical and biological sensors [19–21], and high-density optical data recording materials [22,23], have been developed by exploring optical responses of self-assembled colloidal photonic crystals. The peak positions of photonic band gaps (or more precisely, optical stop bands) of 3-D colloidal photonic crystals are governed by the Bragg diffraction equation: $\lambda_{\text{peak}} = 2 \times n_{\text{eff}} \times d \times \sin \theta$, where n_{eff} is the effective refractive index of the diffractive medium, d is the inter-plane distance, and θ is the light incident angle. By tuning the effective refractive index and/or the inter-plane distance through different mechanisms [24–35], such as solvent swelling, mechanical deformation, and applying external electrical and magnetic fields, tunable photonic crystals devices (e.g., full color displays and photonic papers) have been demonstrated [36–40].

Self-assembled photonic crystals [41–52], such as 1-D titania/silica multilayers and 2-D porous silicon, have also been widely used in sensitive vapor detection. The concentration of vapors can be deduced by monitoring the change of optical properties, such as wavelength shift of the optical stop bands or the Fabry–Perot fringes of the diffractive media during vapor condensation. 3-D photonic crystals, such as blue-colored *Morpho* butterfly wing scales which exhibit unusual optical diffraction and interference, have recently been demonstrated for highly selective vapor detection [53]. Unfortunately, the limited material selection of these natural 3-D photonic crystals and the irreversible structural change induced by certain vapors impede the development of reproducible and reusable vapor sensors that can be operated over a wide range of temperatures. Self-assembled 3-D colloidal photonic crystals have also been investigated for vapor sensing. Polymer embedded colloidal crystals are frequently used to maximize the wavelength shift of the Bragg diffraction peaks [52,54], though swelling of the polymer matrix instead of capillary condensation of condensable vapors is the mechanism for vapor sensing. The absorption of chemical species in mesoporous synthetic opals has been studied and the condensation of vapors occurs mostly in the mesopores of the microspheres [55]. The capillary condensation of vapors in layer-by-layer assembled nanoparticle thin films has also been interrogated to facilitate the fabrication of heterostructured thin films with modulated refractive index profiles [56].

Here we report the sensitive and reversible detection of vapors by using self-assembled 3-D colloidal photonic crystals. Colloidal silica photonic crystals prepared by a convective self-assembly

* Corresponding author. Fax: +1 352 392 9513.

E-mail address: pjiang@che.ufl.edu (P. Jiang).

technology are used in the current work [6]. Compared to macroporous polymer vapor detectors which have been described in our recent publication [57], the good chemical resistance, negligible solvent swelling, and high thermal stability of silica microspheres enable the detection of a large variety of polar and nonpolar vapors over a wide range of operating temperatures. However, the lower volume fraction of voids in self-assembled colloidal crystals (~ 0.26) than that of templated macroporous polymer membranes (~ 0.74) reduces the amount of condensed vapors in the diffractive media and thus affects the detection sensitivity. We have therefore developed a novel full-peak analysis technique that improves the detection sensitivity by nearly two orders of magnitude. Most importantly, the condensation of vapors in between submicrometer-scale microspheres, a topic that has received little examination while has important technological applications (e.g., in creating broadband antireflection coatings) [56,58], has also been systematically investigated by both experiments and theoretical calculations.

2. Experimental

2.1. Materials and substrates

The reagents used for the synthesis of silica microspheres including tetraethyl orthosilicate (TEOS, 98%) and ammonium hydroxide (28%) were purchased from Sigma–Aldrich. Ethanol (200-proof) was obtained from Pharmaco Products. All solvents and chemicals were of reagent quality and were used without further purification except for TEOS, which was freshly distilled before use. Glass microslides and scintillation vials (Fisher) were cleaned in a “Piranha” solution (a 3:1 mixture of concentrated sulfuric acid with 30% hydrogen peroxide) for half an hour, rinsed with Milli-Q water (18.2 M Ω cm), and dried in a stream of nitrogen.

2.2. Instrumentation

Scanning electron microscopy (SEM) was carried out on a JEOL 6335F FEG-SEM. A thin layer of gold was sputtered onto the samples prior to imaging. Normal incidence optical reflection spectra were obtained using an Ocean Optics HR4000 High Resolution Fiber Optic Vis-near-IR spectrometer with a reflection probe.

2.3. Preparation of colloidal photonic crystals by convective self-assembly

The synthesis of monodispersed silica microspheres with less than 5% diameter standard deviation was performed by following the Stöber method [59]. The as-synthesized silica microspheres were purified by multiple centrifugation/re-dispersion cycles (at least four times) in 200-proof ethanol. The final particle volume fraction of colloidal suspensions was adjusted to 1%. A clean glass microslide was placed vertically into 15 mL of purified silica alcohol contained in a scintillation vial. The vial was covered by a crystallizing dish to keep out external airflow and contamination. The entire apparatus was placed on a vibration-free bench in a temperature-controlled laboratory (22 ± 1 °C). The spontaneous crystallization of silica microspheres at a meniscus between the vertical substrate and the colloidal suspension led to the formation of highly ordered colloidal photonic crystals as the meniscus was slowly swept across the substrate by solvent evaporation [6].

2.4. Experimental apparatus and procedures for vapor detection

The self-assembled silica colloidal photonic crystal was placed horizontally in a home-made environmental chamber. The chamber

was evacuated and then back-filled with a condensable vapor with a specific pressure (measured by a Fisher diaphragm vacuum gauge). Dry nitrogen was used to control the total pressure of the chamber to be 1 atm. A reflection probe connected to an Ocean Optics Vis-near-IR spectrometer was sealed in the environmental chamber to measure the specular optical reflectance from the colloidal photonic crystal. A calibrated halogen light source was used to illuminate the sample. The beam spot size was about 3 mm on the sample surface. Measurements were performed at normal incidence and the cone angle of collection was less than 5°. Absolute reflectivity was obtained as the ratio of the sample spectrum and a reference spectrum. The reference spectrum was the optical density obtained from an aluminum-sputtered (1000 nm thickness) silicon wafer.

3. Results and discussion

The colloidal photonic crystals used for the vapor sensing experiments were prepared by the convective self-assembly technology [6]. Planar colloidal single crystals with tunable thickness can be easily assembled over centimeter-sized areas on various substrates by using this methodology. Fig. 1a shows a top-view SEM image of a silica colloidal crystal consisting of 260 nm diameter microspheres. The sample exhibits an hexagonally ordered, close-packed arrangement of silica spheres over a sample area of 50 μm^2 which indeed extends over the whole sample surface. While order within the (111) plane parallel to the substrate is important, the stacking of close-packed layers perpendicular to the substrate is responsible for the optical diffraction observed in normal-incidence reflectance measurements. Colloid crystal films were thus abraded to reveal the stacking perpendicular to the substrate as shown in Fig. 1b. This

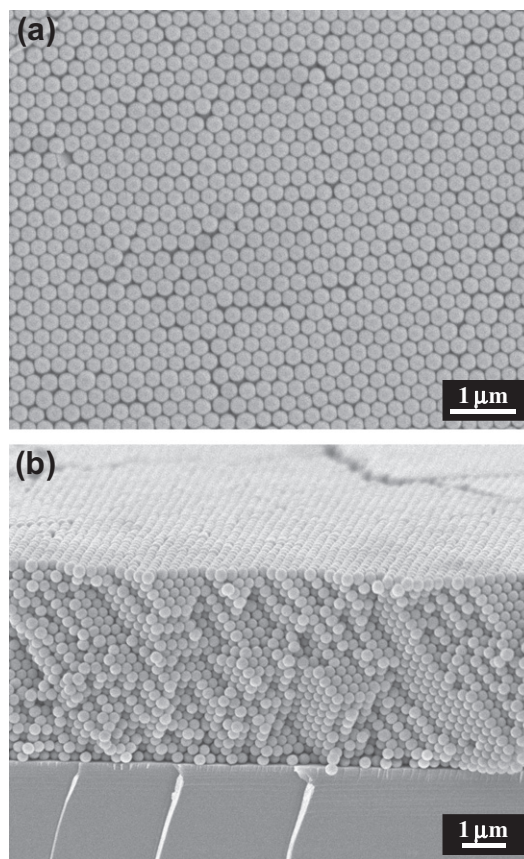


Fig. 1. SEM images of a colloidal photonic crystal consisting of 260 nm silica microspheres fabricated by convective self-assembly. (a) Top-view and (b) side-view.

cross-sectional SEM image shows that the close-packed structure extends uniformly over 20 colloidal layers. Although the convectively assembled colloidal crystals are single crystals (as evidenced by the uniform diffractive color and the unidirectional crystallographic orientation), common defects such as cracks and point defects are observed routinely in SEM images.

The self-assembled colloidal photonic crystal was placed horizontally in a home-made environmental chamber and then exposed to a condensable vapor with a specific partial pressure. Dry nitrogen was used to control the total pressure of the chamber to be 1 atm. The normal incidence specular reflectance spectra from the colloidal photonic crystal were obtained by using an *in situ* Vis-near-IR spectrometer. By monitoring the time dependence of the specular reflectance spectra at different sensing conditions (e.g., different vapor partial pressures and temperatures), we found that the condensation equilibrium was reached in less than 1 min for all conditions used in this work. Fig. 2a shows the reflectance spectra obtained from a colloidal photonic crystal consisting of 260 nm silica microspheres exposed to ethanol vapors with different partial pressures (from $0.1P_0$ to $1.0P_0$) at $70 \pm 1^\circ\text{C}$. P_0 is the saturation vapor pressure of ethanol at this temperature. All spectra display distinct Bragg diffraction peaks with well-defined Fabry–Perot fringes, indicating high crystalline quality of the self-assembled colloidal photonic crystals. When the partial pressure of ethanol vapor was increased, ethanol condensed in the interstitials between the close-packed silica microspheres, leading to a higher effective refractive index of the diffractive medium and a smaller dielectric contrast between

the silica spheres and the surrounding medium. This leads to the observed red-shift of the Bragg diffraction peaks and the reduction of the amplitude of the optical stop bands as shown in Fig. 2a [60]. The optical properties of the colloidal photonic crystals were fully recovered when the condensed ethanol was evaporated. The photonic crystal films can thus be reused many times for reproducible vapor detection.

The principle of colloidal photonic crystal vapor detectors is to monitor the wavelength shift of the diffraction peaks ($\Delta\lambda_{\text{peak}}$) when the samples are exposed to different environment. Thus a linear response of $\Delta\lambda_{\text{peak}}$ vs. vapor partial pressure is crucial for determining the vapor contents. Fig. 2b shows that the shift of the zeroth-order Bragg diffraction peaks (compared to the control sample exposed to pure nitrogen gas) is nearly linear with ethanol partial pressure. The maximum wavelength shift of ~ 10 nm was achieved when the colloidal photonic crystal was exposed to a saturated ethanol vapor. Similar maximum wavelength shift was obtained for other saturated vapors (e.g., water and toluene). This indicates that the detection sensitivity of colloidal photonic crystal-based vapor detectors is ~ 10 nm per saturation vapor pressure unit (P_0). To significantly improve the detection sensitivity, we developed a novel full-peak analysis technology which takes advantage of the manifest amplitude reduction of the Bragg diffraction peaks during vapor condensation. Instead of using the conventional method for merely monitoring the small peak shift, we calculated the integrated response of the zeroth-order Bragg diffraction peak by using the integration tool of the OriginPro 8.5 software which can automatically determine the peak range of the diffraction peak. The well-defined Fabry–Perot fringes also enable manual picking of the range of the zeroth-order Bragg diffraction peak. It is worthy to mention that full-peak analysis is commonly used in other detection methods, for example, IR spectroscopic sensors, gas chromatography, and many others. Our full-peak analysis method can be easily used for self-assembled photonic crystals with more than 3–4 colloidal monolayers which show distinct zeroth-order Bragg diffraction peak and Fabry–Perot fringes [60]. Fig. 2b shows that the integrated response of the zeroth-order diffraction peaks from the (1 1 1) lattice planes is also linear with ethanol partial pressure. The integrated response of the colloidal photonic crystal exposed to pure nitrogen gas and saturated ethanol vapor is 2410 ± 18 nm and 1715 ± 13 nm, respectively. This corresponds to a detection sensitivity of 695 nm per saturation vapor pressure unit, which is almost two orders of magnitude higher than that obtained by the conventional peak-shift analysis technique.

Compared to macroporous polymer vapor detectors [57], the good chemical resistance and negligible solvent swelling of silica microspheres enable the reversible and reproducible detection of a large variety of vapors ranging from water to toluene. Fig. 3a shows that the optical response of water vapor detection at $90 \pm 1^\circ\text{C}$ is quite similar to that of ethanol detection as shown in Fig. 2a. The results in Fig. 3b indicate that a 9 nm wavelength shift and a 705 nm difference in integrated response can be achieved when the silica colloidal crystal is exposed to saturated water vapor. Not only polar vapors, the colloidal photonic crystals can also be utilized to detect nonpolar vapors. Fig. 4 presents the results of toluene vapor detection at $100 \pm 1^\circ\text{C}$. The good linear relationship of the peak shift and the integrated response vs. the toluene partial pressure is clearly illustrated by Fig. 4b. The higher refractive index of toluene (~ 1.50) than that of ethanol (~ 1.36) and water (~ 1.33) leads to a higher effective refractive index of the diffractive medium, resulting in a larger red-shift of the optical stop bands (~ 15 nm) when the colloidal photonic crystal was exposed to a saturated toluene vapor.

To gain a better understanding of condensation of condensable vapors in self-assembled colloidal photonic crystals, we calculated the amount of the condensed liquids at different vapor partial

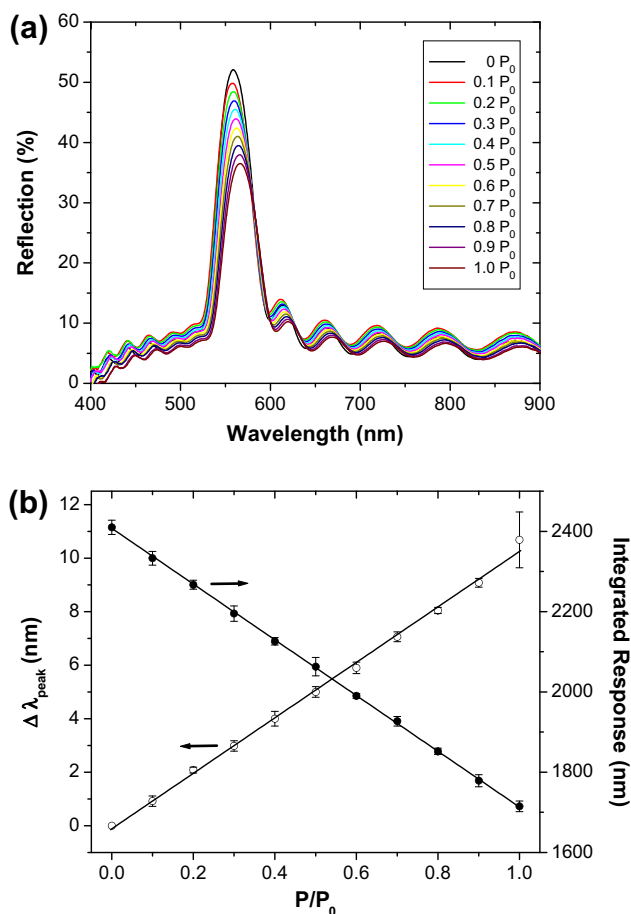


Fig. 2. (a) Normal-incidence specular reflection spectra obtained from a colloidal crystal consisting of 260 nm silica microspheres exposed to ethanol vapors with different partial pressures. (b) Dependence of the shift and the integrated response of the zeroth-order Bragg diffraction peak vs. ethanol partial pressure.

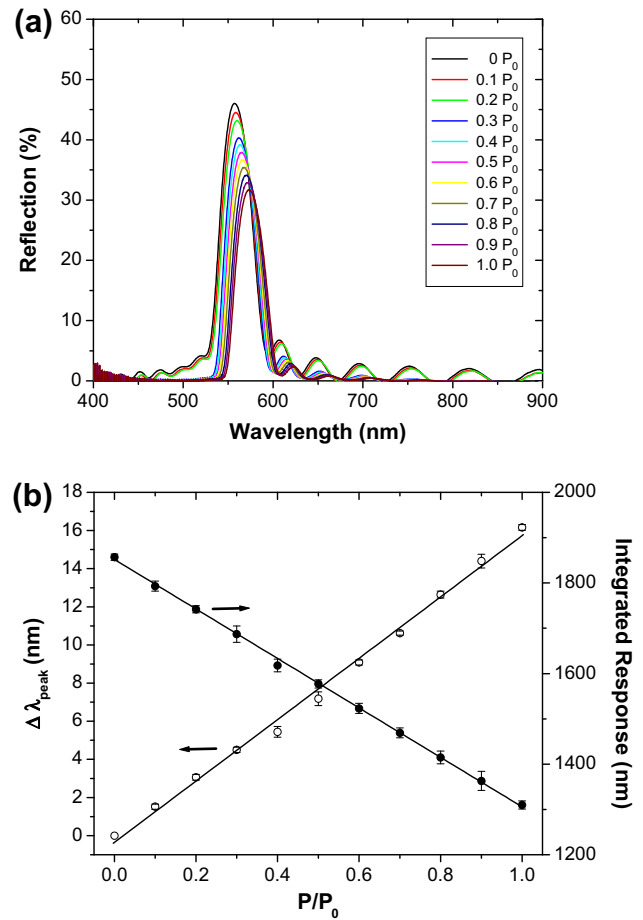
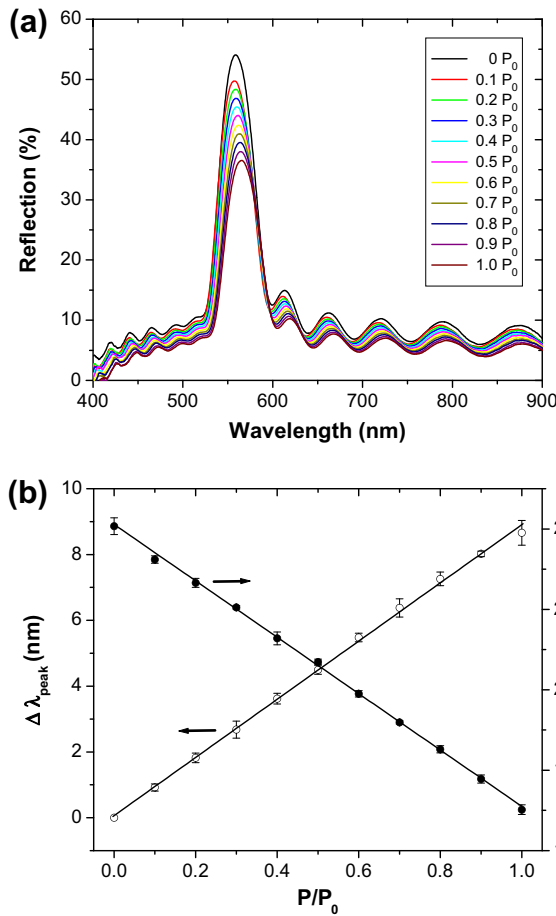


Fig. 3. (a) Normal-incidence specular reflection spectra obtained from a colloidal crystal consisting of 260 nm silica microspheres exposed to water vapors with different partial pressures and (b) dependence of the shift and the integrated response of the zeroth-order Bragg diffraction peak vs. water partial pressure.

Fig. 4. (a) Normal-incidence specular reflection spectra obtained from a colloidal crystal consisting of 260 nm silica microspheres exposed to toluene vapors with different partial pressures and (b) dependence of the shift and the integrated response of the zeroth-order Bragg diffraction peak vs. toluene partial pressure.

pressures by using the Bragg diffraction equation. By assuming perfect close-packing of silica microspheres and the volume fraction (VF) of silica and air in a dry colloidal crystal film is 0.74 and 0.26, respectively, the effective refractive index of the colloidal photonic crystal with the condensed liquid can be calculated as: $n_{\text{eff}} = n_{\text{silica}} \times 0.74 + n_{\text{air}} \times (0.26 - VF_{\text{liquid}}) + n_{\text{liquid}} \times VF_{\text{liquid}}$, where VF_{liquid} is the volume fraction of the condensed liquid, n_{silica} , n_{air} , and n_{liquid} are refractive index of silica microspheres (1.42), air (1.0), and condensed liquid, respectively. The calculated volume fractions of the condensed liquids including water, ethanol, and toluene at different vapor partial pressures are shown in Fig. 5. It is apparent that the condensed liquids only partially filled the interstitials between silica microspheres even when the vapors were saturated. For instance, only $\sim 29\%$ of void space between silica microspheres was occupied by toluene when the colloidal photonic crystal was exposed to a saturated toluene vapor at 100 °C. In Fig. 5, the volume fraction of the condensed toluene is higher than that of ethanol and water. This is because the partial pressure of toluene at the operating temperature (100 °C) is higher than that of ethanol (operating at 70 °C) and water (operating at 90 °C). For example, the saturated vapor pressure of toluene, ethanol, and water at the above temperatures is 559.5, 541.2, and 525.76 mm Hg, respectively [61].

The calculated volume fractions of the condensed liquids were then incorporated in the scalar wave approximation (SWA) model [60,62] developed for periodic dielectric structures to quantitatively simulate the specular reflectance spectra at different vapor partial pressures. Fig. 6a, c, and e shows the simulated optical

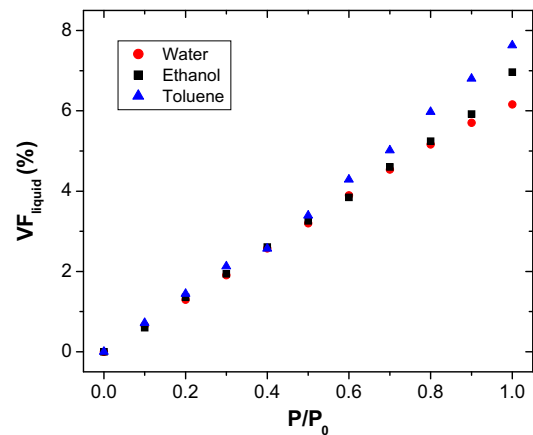


Fig. 5. Calculated volume fractions of condensed ethanol, water, and toluene at different vapor partial pressures.

reflection spectra for ethanol, water, and toluene at different vapor partial pressures. Although the simulated spectra exhibit slightly higher reflectance than the experimental results (compare with Figs. 2a, 3a, and 4a), the shape, position, red-shift, and amplitude reduction of the diffractive peaks associated with the condensation of vapors in the voids of colloidal photonic crystals agree well with the experiments. The remarkable agreement between theory and experiment further confirms the high crystalline quality of the

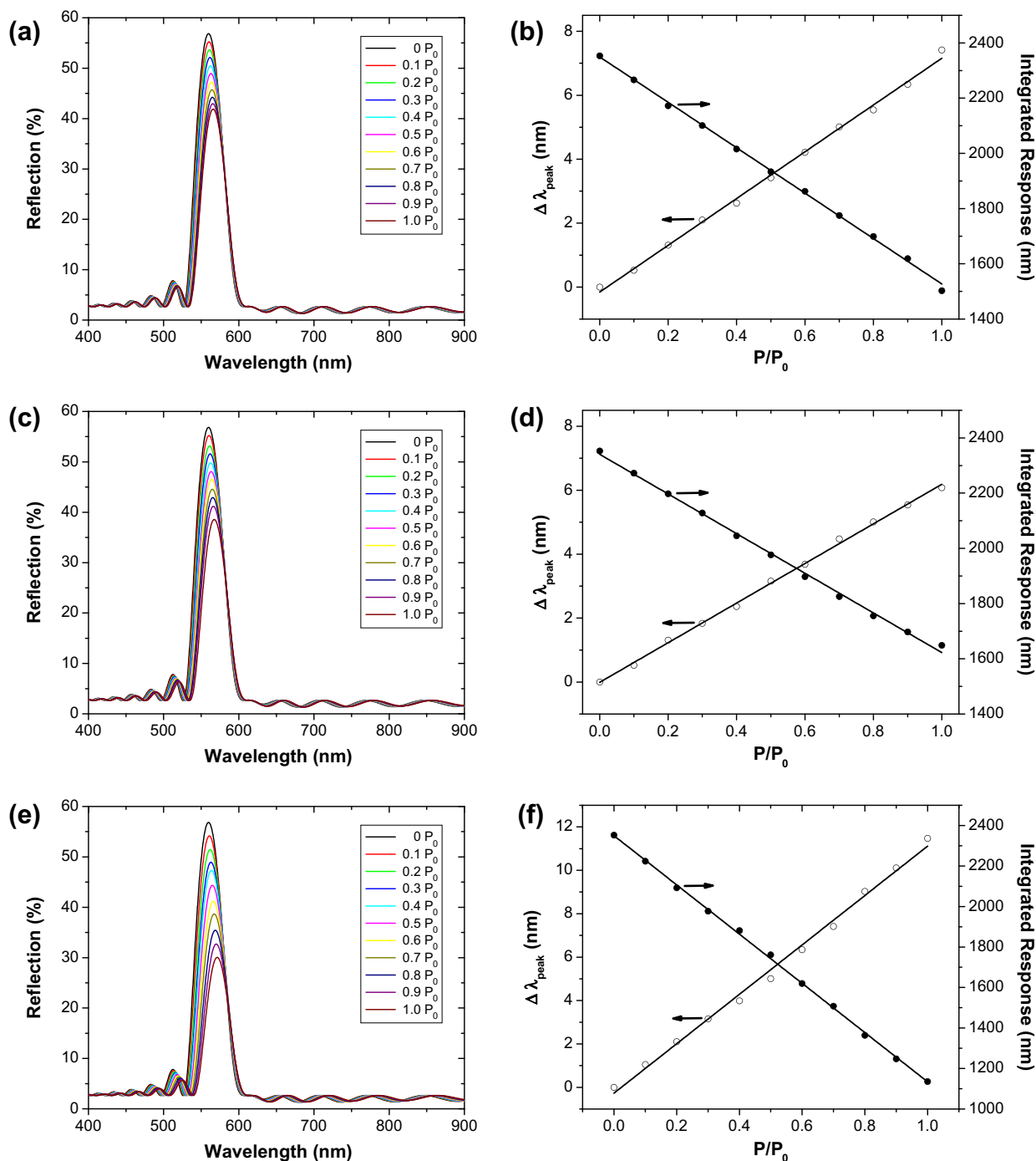


Fig. 6. Simulated specular reflection spectra and calculated shift and integrated response of the zeroth-order Bragg diffraction peak vs. vapor partial pressure obtained from colloidal crystals consisting of 260 nm silica microspheres exposed to condensable vapors at different vapor pressures. (a and b) Ethanol vapor. (c and d) Water vapor. (e and f) Toluene vapor.

convectively self-assembled colloidal photonic crystals and validates the calculated volume fractions of the condensed liquids by using the Bragg diffraction equation.

Using the simulated specular reflectance spectra, we further calculated the shift and integrated response of the zeroth-order Bragg diffraction peak at different vapor partial pressures and the results are shown in Fig. 6b, d, and e for ethanol, water, and toluene, respectively. The good linear relationship of the peak shift and the integrated response vs. vapor partial pressure is clearly shown. The calculated detection sensitivity based on $\Delta\lambda_{\text{peak}}$ is 7.4, 6.1, and 11.5 nm per saturation vapor pressure unit for ethanol, water and

toluene; while a much improved sensitivity of 850, 704, and 1217 nm per saturation vapor pressure unit is obtained by using integrated response. The calculated sensitivity is lower than that of experimental sensitivity based on $\Delta\lambda_{\text{peak}}$ (10.6, 8.6, and 16.1 nm per saturation vapor pressure unit for ethanol, water, and toluene vapors) and higher than that of experimental sensitivity based on integrated response (695, 705, and 547 nm per saturation vapor pressure unit). The intrinsic defects (e.g., vacancies, line defects, and cracks) of the self-assembled colloidal crystals could lead to higher adsorption and condensation of vapors. This will increase the effective refractive index of the diffractive medium and thus

results in a larger experimental peak shift (i.e., higher $\Delta\lambda_{\text{peak}}$ -based sensitivity). By contrast, the intrinsic defects of colloidal photonic crystals could significantly reduce the amplitude of the Bragg diffraction peaks [63] and therefore lead to lower experimental sensitivity based on integrated response.

The condensation of vapors in colloidal photonic crystals is possibly caused by capillary condensation. The modified Kelvin equation [56,64],

$$\ln \frac{P}{P_0} = \frac{\gamma V_l}{RT} \left(\frac{1}{x} - \frac{1}{r_c} \right) \quad (1)$$

where P and P_0 are actual and saturation vapor pressure, γ is the liquid/vapor surface tension, V_l is the liquid molar volume, R is the universal gas constant, T is the absolute temperature, x and r_c are two principal radii characterizing the saddle-shaped liquid–vapor interface (see Fig. 7a), can be used to describe the phenomenon of capillary condensation of a condensable vapor in between two touching microspheres. To calculate x and r_c at different vapor partial pressures, we set up a xy coordinate system with point C as the origin, and CO_1, CO_3 as the x, y axis, respectively (Fig. 8(a)). Applying Pythagorean Theorem for the right triangle CO_1O_3 yields: $(r_c + x)^2 + r^2 = (r_c + r)^2$. Therefore, x can be expressed by r and r_c as follows:

$$x = \sqrt{2rr_c + r_c^2} - r_c \quad (2)$$

Under the above coordinate system, the center of the three spheres O_1, O_2, O_3 (O_3 is a virtual sphere) and the intersection points A – C have the following coordinate values:

$$O_1 = (r, 0), \quad O_2 = (-r, 0), \quad O_3 = \left(0, \sqrt{2rr_c + r_c^2} \right)$$

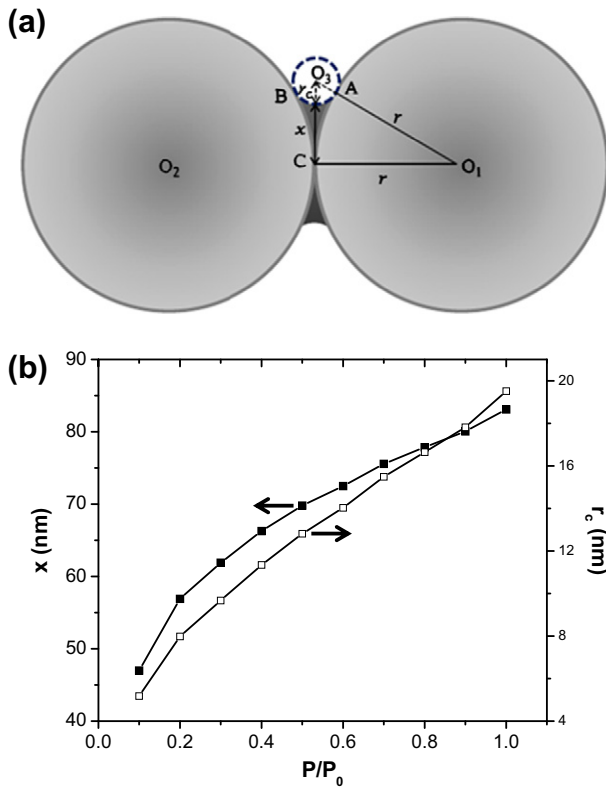


Fig. 7. (a) Scheme of the capillary condensation of a vapor between two touching spheres and (b) dependence of the two principal radii [x and r_c in (a)] characterizing the saddle-shaped condensed ethanol–air interface vs. ethanol partial pressure.

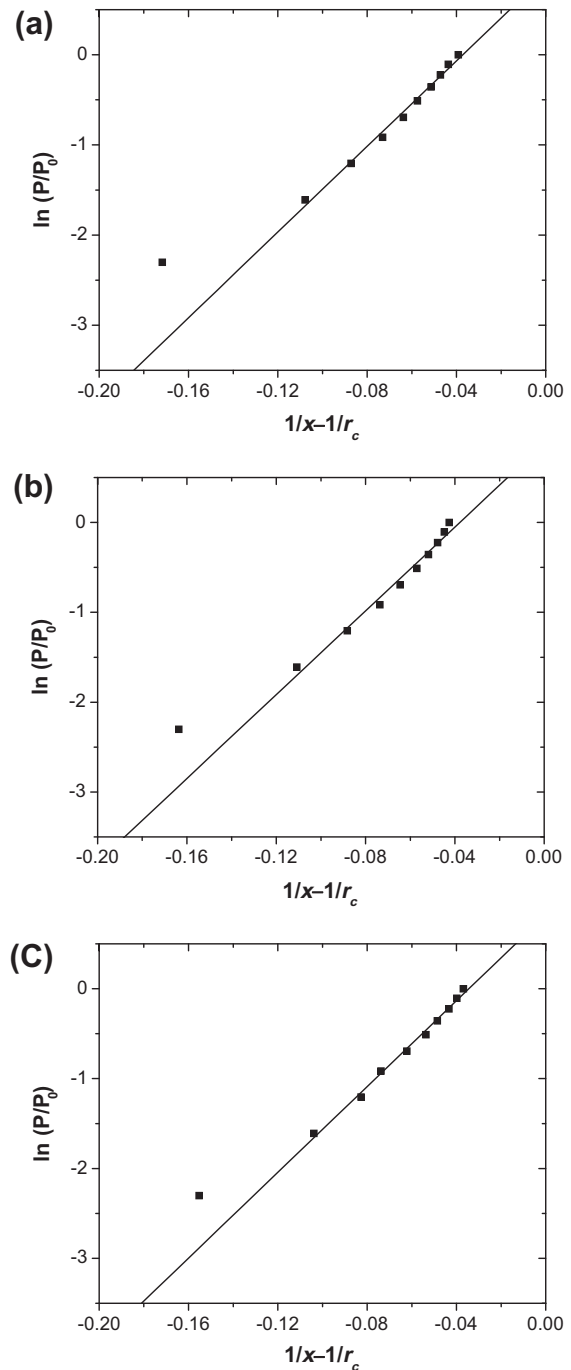


Fig. 8. Dependence of $\ln(P/P_0)$ vs. the difference of the reciprocal of the two principal radii characterizing the saddle-shaped condensed vapor–air interface. (a) Ethanol vapor, (b) water vapor, and (c) toluene vapor.

$$A = \left(\frac{rr_c}{r+r_c}, \frac{r\sqrt{2rr_c+r_c^2}}{r+r_c} \right) \quad B = \left(-\frac{rr_c}{r+r_c}, \frac{r\sqrt{2rr_c+r_c^2}}{r+r_c} \right), \quad C = (0, 0)$$

The condensed liquid between spheres O_1 and O_2 can be approximated by revolution of the arc BA around x -axis. The equation of the arc BA can be expressed by

$$y = \sqrt{2rr_c + r_c^2} - \sqrt{r_c^2 - x^2}$$

where $-\frac{rr_c}{r+r_c} \leq x \leq \frac{rr_c}{r+r_c}$. The volume $V_{O_1O_2}$ of the liquid between spheres O_1 and O_2 can then be computed as a definite integral

$$V_{O_1O_2} = \int_{-\frac{\pi r_c}{r+r_c}}^{\frac{\pi r_c}{r+r_c}} \pi \left(\sqrt{2rr_c + r_c^2} - \sqrt{r_c^2 - x^2} \right)^2 dx \quad (3)$$

Putting Eq. (2) into (3), we can see that $V_{O_1O_2}$ is clearly a function of r_c while r is a constant (sphere radius). Since the sphere O_1 has 12 close-packed neighboring spheres while it only possesses half of the volume $V_{O_1O_2}$ for each neighbor, the ratio between volumes of the condensed liquid and the spheres can be computed by

$$\text{ratio} = \frac{12 \times \frac{V_{O_1O_2}}{2}}{\frac{4}{3} \pi r^3} \quad (4)$$

which is surely a function of r_c . Under Matlab computing environment, we wrote a program [65] to solve the associated r_c value for each ratio obtained from experiment based on Eq. (4); then computed the corresponding x value from Eq. (2).

The calculated r_c and x values for condensed ethanol between 260 nm silica microspheres at different ethanol partial pressures are plotted in Fig. 7b. For instance, x of 83.1 nm and r_c of 19.5 nm were obtained for saturated ethanol vapor. The calculated r_c and x values were then used to calculate $\left(\frac{1}{x} - \frac{1}{r_c}\right)$. As shown by Eq. (1), $\ln \frac{p}{p_0}$ should be proportional to $\left(\frac{1}{x} - \frac{1}{r_c}\right)$ at a fixed temperature because γ (17.98 mN/m), V_1 (61.67 cm³), R (8.314 J/(mol K)) and T (343.15 K) are all constants. Fig. 8 shows that this prediction agrees well with experimental results for ethanol, water, and toluene for a wide range of vapor partial pressures (from 0.2 P_0 to 1.0 P_0). A large deviation is observed when the vapor partial pressure is low. As only a very small fraction of voids between self-assembled microspheres is occupied by the condensed liquid at low vapor partial pressure, the two principal radii and the saddle-shaped liquid-vapor interface may not be well defined. A relatively large change in x and r_c values between 0.1 P_0 and 0.2 P_0 has been observed for all three vapors (e.g., see Fig. 7b)). This could be the reason for the large discrepancy between the experiments and theoretical predictions at low vapor pressures.

The capillary condensation and evaporation (or adsorption and desorption) of condensable vapors in porous systems with various pore sizes and shapes have been well studied and five types of adsorption isotherms have been documented [66–69]. The processes of condensation and evaporation do not necessarily take place as exact reverses of each other, leading to the formation of hysteresis in types I, IV and V adsorption isotherms [69]. In addition, typical adsorption isotherms are usually quasi-linear only at relatively low vapor partial pressures (<0.5 P_0). However, in our self-assembled colloidal crystals consisting of submicrometer-sized microspheres, which is a porous system that has received little examination, the adsorption isotherms (Fig. 5) are quasi-linear for the whole range of vapor partial pressure from 0 to P_0 . Additionally, our experiments show that no hysteresis exists between the adsorption and desorption processes. Within experimental errors, we found that the shape and position of Bragg diffraction peaks are completely reversible during cycling vapor condensation and evaporation.

As shown above, the observed condensation of vapors match reasonably well with the modified Kelvin equation when a simplified model consisting of close-packed equal-sized microspheres is used. As illustrated in Fig. 7a, condensation could be nucleated by the adsorbed liquid in the crevices between the touching spheres to give a torus of liquid which, as pressure increases, could extend inwards until adjacent tori coalesce. As shown by the adsorption isotherms in Fig. 5, only a small fraction (<29%) of the interstitial space between silica microspheres is filled with the condensed liquid even when the vapor is saturated. Therefore the majority of the spherical cavity is empty during the vapor condensation and evaporation processes and the condensed liquid forms nearly isolated, cone-shaped menisci between touching

microspheres. The process of evaporation can then be the exact reverse of that of condensation, and hysteresis is therefore absent. This behavior is very similar to that exhibited by cone-shaped and wedge-like porous systems [69]. The linear adsorption isotherm over a wide range of vapor partial pressures shown by the self-assembled colloidal crystals is also related to the relatively low adsorption amount. Linear adsorption regions have been observed for types II and IV isotherms when the adsorbed amount is not high [69]. However, we are not excluding the possibility of a simple adsorption of vapors on hydrophilic silica particles, especially considering no hysteresis and quasi-linearity exhibited by our self-assembled colloidal systems (Fig. 5).

4. Conclusions

In conclusion, we have demonstrated that 3-D colloidal photonic crystals created by the convective self-assembling technology can be used as sensitive vapor detectors for a variety of vapors. The detection sensitivity can be greatly improved by using a new full-peak analysis technique, which can be extended to other types of optical sensors, such as surface-plasmon resonance (SPR) sensors that also monitor the small shift of SPR peaks [70]. The adjustable filling of the interstitials of colloidal photonic crystals could facilitate the design and fabrication of tunable optical devices that have important technological applications ranging from full color displays to broadband antireflection coatings.

Acknowledgments

This work was supported in part by DTRA and NSF under Grant No. CBET-0744879 and CMMI-1000686.

Appendix A. Supplementary material

Supplementary data associated with this article can be found, in the online version, at doi:10.1016/j.jcis.2011.12.058.

References

- [1] J.D. Joannopoulos, R.D. Meade, J.N. Winn, *Photonic Crystals: Molding the Flow of Light*, Princeton University Press, Princeton, 1995.
- [2] J.D. Joannopoulos, P.R. Villeneuve, S.H. Fan, *Nature* 386 (1997) 143.
- [3] A. van Blaaderen, R. Ruel, P. Wiltzius, *Nature* 385 (1997) 321.
- [4] R. Mayoral, J. Requena, J.S. Moya, C. Lopez, A. Cintas, H. Miguez, F. Meseguer, L. Vazquez, M. Holgado, A. Blanco, *Adv. Mater.* 9 (1997) 257.
- [5] S.H. Park, Y.N. Xia, *Langmuir* 15 (1999) 266.
- [6] P. Jiang, J.F. Bertone, K.S. Hwang, V.L. Colvin, *Chem. Mater.* 11 (1999) 2132.
- [7] Y.A. Vlasov, X.Z. Bo, J.C. Sturm, D.J. Norris, *Nature* 414 (2001) 289.
- [8] S. Wong, V. Kitaev, G.A. Ozin, *J. Am. Chem. Soc.* 125 (2003) 15589.
- [9] B.G. Prevo, O.D. Velev, *Langmuir* 20 (2004) 2099.
- [10] P. Jiang, M.J. McFarland, *J. Am. Chem. Soc.* 126 (2004) 13778.
- [11] C.I. Aguirre, E. Reguera, A. Stein, *Adv. Funct. Mater.* 20 (2010) 2565.
- [12] J.P. Ge, Y.D. Yin, *Angew. Chem., Int. Ed.* 50 (2011) 1492.
- [13] O. Sato, S. Kubo, Z.Z. Gu, *Acc. Chem. Res.* 42 (2009) 1.
- [14] Z.Z. Gu, H. Uetsuka, K. Takahashi, R. Nakajima, H. Onishi, A. Fujishima, O. Sato, *Angew. Chem., Int. Ed.* 42 (2003) 894.
- [15] S.H. Kim, H.S. Park, J.H. Choi, J.W. Shim, S.M. Yang, *Adv. Mater.* 22 (2010) 946.
- [16] J.M. Weissman, H.B. Sunkara, A.S. Tse, S.A. Asher, *Science* 274 (1996) 959.
- [17] A. Blanco, E. Chomski, S. Grzybchak, M. Ibisate, S. John, S.W. Leonard, C. Lopez, F. Meseguer, H. Miguez, J.P. Mondia, G.A. Ozin, O. Toader, H.M. van Driel, *Nature* 405 (2000) 437.
- [18] S.H. Kim, W.C. Jeong, S.M. Yang, *Chem. Mater.* 21 (2009) 4993.
- [19] O.D. Velev, E.W. Kaler, *Langmuir* 15 (1999) 3693.
- [20] J.H. Holtz, S.A. Asher, *Nature* 389 (1997) 829.
- [21] S.A. Asher, V.L. Alexeev, A.V. Goponenko, A.C. Sharma, I.K. Lednev, C.S. Wilcox, D.N. Finegold, *J. Am. Chem. Soc.* 125 (2003) 3322.
- [22] H.H. Pham, I. Gourevich, J.K. Oh, J.E.N. Jonkman, E. Kumacheva, *Adv. Mater.* 16 (2004) 516.
- [23] B.J. Siwick, O. Kalinina, E. Kumacheva, R.J.D. Miller, J. Noolandi, *J. Appl. Phys.* 90 (2001) 5328.
- [24] J.D. Debord, L.A. Lyon, *J. Phys. Chem. B* 104 (2000) 6327.
- [25] L.L. Duan, B. You, L.M. Wu, M. Chen, *J. Colloid Interface Sci.* 353 (2011) 163.
- [26] Y. Iwayama, J. Yamanaka, Y. Takiguchi, M. Takasaka, K. Ito, T. Shinohara, T. Sawada, M. Yoneda, *Langmuir* 19 (2003) 977.

- [27] H. Kim, J. Ge, J. Kim, S. Choi, H. Lee, W. Park, Y. Yin, S. Kwon, *Nature Photon.* 3 (2009) 534.
- [28] J. Li, W.H. Huang, Y.C. Han, *Colloid Surf. A* 279 (2006) 213.
- [29] S.H. Foulger, P. Jiang, A. Lattam, D.W. Smith, J. Ballato, D.E. Dausch, S. Grego, B.R. Stoner, *Adv. Mater.* 15 (2003) 685.
- [30] D. Suzuki, J.G. McGrath, H. Kawaguchi, L.A. Lyon, *J. Phys. Chem. C* 111 (2007) 5667.
- [31] J.X. Wang, Y.Q. Wen, H.L. Ge, Z.W. Sun, Y.M. Zheng, Y.L. Song, L. Jiang, *Macromol. Chem. Phys.* 207 (2006) 596.
- [32] W. Wohlleben, F.W. Bartels, S. Altmann, R.J. Leyrer, *Langmuir* 23 (2007) 2961.
- [33] L. Xu, J.X. Wang, Y.L. Song, L. Jiang, *Chem. Mater.* 20 (2008) 3554.
- [34] A. Yethiraj, *Soft Matter* 3 (2007) 1099.
- [35] T.S. Shim, S.H. Kim, J.Y. Sim, J.M. Lim, S.M. Yang, *Adv. Mater.* 22 (2010) 4494.
- [36] A.C. Arsenault, T.J. Clark, G. Von Freymann, L. Cademartiri, R. Sapienza, J. Bertolotti, E. Vekris, S. Wong, V. Kitaev, I. Manners, R.Z. Wang, S. John, D. Wiersma, G.A. Ozin, *Nat. Mater.* 5 (2006) 179.
- [37] A.C. Arsenault, D.P. Puzzo, A. Ghoussoub, I. Manners, G.A. Ozin, *J. Soc. Info. Display* 15 (2007) 1095.
- [38] A.C. Arsenault, D.P. Puzzo, I. Manners, G.A. Ozin, *Nat. Photonics* 1 (2007) 468.
- [39] H. Fudouzi, Y.N. Xia, *Langmuir* 19 (2003) 9653.
- [40] J.Y. Huang, X.D. Wang, Z.L. Wang, *Nano Lett.* 6 (2006) 2325.
- [41] N. Hidalgo, M.E. Calvo, S. Colodrero, H. Miguez, *IEEE Sens. J.* 10 (2010) 1206.
- [42] S.Y. Choi, M. Mamak, G. von Freymann, N. Chopra, G.A. Ozin, *Nano Lett.* 6 (2006) 2456.
- [43] M.S. Salem, M.J. Sailor, F.A. Harraz, T. Sakka, Y.H. Ogata, *J. Appl. Phys.* 100 (2006).
- [44] L. De Stefano, L. Moretti, A. Lamberti, O. Longo, M. Rocchia, A.M. Rossi, P. Arcari, I. Rendina, *IEEE Trans. Nanotechnol.* 3 (2004) 49.
- [45] X.Y. Fang, V.K.S. Hsiao, V.P. Chodavarapu, A.H. Titus, A.N. Cartwright, *IEEE Sens. J.* 6 (2006) 661.
- [46] T. Karacali, M. Alanyalioglu, H. Efeoglu, *IEEE Sens. J.* 9 (2009) 1667.
- [47] B.H. King, A. Gramada, J.R. Link, M.J. Sailor, *Adv. Mater.* 19 (2007) 4044.
- [48] V.S.Y. Lin, K. Motesharei, K.P.S. Dancil, M.J. Sailor, M.R. Ghadiri, *Science* 278 (1997) 840.
- [49] A.M. Ruminski, M.M. Moore, M.J. Sailor, *Adv. Funct. Mater.* 18 (2008) 3418.
- [50] H. Saha, C. Pramanik, *Mater. Chem. Phys.* 21 (2006) 239.
- [51] G.G. Salgado, T.D. Becerril, H.J. Santiesteban, E.R. Andres, *Opt. Mater.* 29 (2006) 51.
- [52] A.C. Arsenault, V. Kitaev, I. Manners, G.A. Ozin, A. Mihi, H. Miguez, *J. Mater. Chem.* 15 (2005) 133.
- [53] R.A. Potyrailo, H. Ghiradella, A. Vertiatchikh, K. Dovidenko, J.R. Cournoyer, E. Olson, *Nat. Photon.* 1 (2007) 123.
- [54] T. Endo, Y. Yanagida, T. Hatsuzawa, *Sens. Actuators B* 125 (2007) 589.
- [55] Y. Yamada, T. Nakamura, K. Yano, *Langmuir* 24 (2008) 2779.
- [56] Z. Gemici, P.I. Schwachulla, E.H. Williamson, M.F. Rubner, R.E. Cohen, *Nano Lett.* 9 (2009) 1064.
- [57] H. Yang, P. Jiang, *Appl. Phys. Lett.* 98 (2011) 011104.
- [58] L.R. Fisher, R.A. Gamble, J. Middlehurst, *Nature* 290 (1981) 575.
- [59] W. Stober, A. Fink, E. Bohn, *J. Colloid Interface Sci.* 26 (1968) 62.
- [60] J.F. Bertone, P. Jiang, K.S. Hwang, D.M. Mittelman, V.L. Colvin, *Phys. Rev. Lett.* 83 (1999) 300.
- [61] D.R. Lide, H.P.R. Frederikse, in: *CRC Handbook of Chemistry and Physics*, 76th ed., CRC Press, Boca Raton, FL, 1995.
- [62] Z. Zhang, S. Satpathy, *Phys. Rev. Lett.* 65 (1990) 2650.
- [63] R. Rengarajan, D. Mittelman, C. Rich, V. Colvin, *Phys. Rev. E* 71 (2005) 016615.
- [64] H.J. Butt, K. Graf, M. Kappl, *Physics and Chemistry of Interfaces*, Wiley-VCH Verlag GmbH, Weinheim, 2006.
- [65] This Matlab Code can be Downloaded from the Online Supplementary Content.
- [66] S. Brunauer, L.S. Deming, W.E. Deming, E. Teller, *J. Am. Chem. Soc.* 62 (1940) 1723.
- [67] A. Grill, V. Patel, K.P. Rodbell, E. Huang, M.R. Baklanov, K.P. Mogilnikov, M. Toney, H.C. Kim, *J. Appl. Phys.* 94 (2003) 3427.
- [68] N. Kunzner, E. Gross, J. Diener, D. Kovalev, V.Y. Timoshenko, D. Wallacher, *J. Appl. Phys.* 94 (2003) 4913.
- [69] S.J. Gregg, K.S.W. Sing, *Adsorption*, second ed., Surface Area and Porosity, Academic Press Inc., London, 1982.
- [70] J. Homola, *Chem. Rev.* 108 (2008) 462.